# An Organizing Center in a Planar Model of Neuronal Excitability

Alessio Franci, Guillaume Drion, Rodolphe Sepulchre

# An Organizing Center in a Planar Model of Neuronal Excitability[*]

## Alessio Franci[†], Guillaume Drion[‡], and Rodolphe Sepulchre[†]

**Abstract.** This paper studies the excitability properties of a generalized FitzHugh–Nagumo model. The model differs from the classical FitzHugh–Nagumo model in that it accounts for the effect of cooperative gating variables such as activation of calcium currents. Excitability is explored by unfolding a pitchfork bifurcation that is shown to organize five different types of excitability. In addition to the three classical types of neuronal excitability, two novel types are described and distinctly associated to the presence of cooperative variables.

**Key words.** neuronal excitability, planar neuron model, bifurcation unfolding, competitive and cooperative variables, voltage-gated calcium channels

**AMS subject classifications.** 92B99, 92C05, 92C42, 37G10

**DOI.** 10.1137/120875016

**1. Introduction.** At the root of neuronal signaling, excitability is a dynamical property shared by all neurons, but its electrophysiological signature largely differs across neurons and experimental conditions. In the early days of experimental neurophysiology, Hodgkin [13] identified three distinct types of excitability (today called Types I, II, and III) by stimulating crustacean nerves with constant current stimuli. The three types of excitability have long been associated to three distinct mathematical signatures in conductance-based models. They all can be described in planar models of the FitzHugh [6] type, which can be rigorously associated to the mathematical reduction of high-dimensional models (see, for instance, the planar reduction of the Hodgkin–Huxley model in [29] and the excitability analysis in [30]). Reduced models have proven central to the understanding of excitability and closely related mechanisms such as bursting. However, understanding excitability in detailed conductance-based models remains a challenge, especially for neurons that exhibit transition between distinctively different firing types depending on environmental conditions. The present paper proposes a generalization of the FitzHugh–Nagumo model that provides novel insights into the simple classification of excitability types.

The proposed model is a "mirrored" version of the FitzHugh–Nagumo model, motivated by the mathematical reduction of conductance-based models including calcium channels. A central observation in [3] is that the electrophysiological signature of excitability is strongly affected by a local property of the recovery variable at the resting equilibrium: if the recovery variable is competitive, that is, provides negative feedback on membrane potential variations

[†]Department of Electrical Engineering and Computer Science, University of Liège, Liège, Belgium (afranci@ulg.ac.be, r.sepulchre@ulg.ac.be).
[‡]Department of Electrical Engineering and Computer Science, and Laboratory of Pharmacology and GIGA Neurosciences, University of Liège, Liège, Belgium (gdrion@ulg.ac.be).

such as in all planar reductions of the Hodgkin–Huxley model, the qualitative properties of excitability are well captured by the classical FitzHugh–Nagumo model. In contrast, if the recovery variable is cooperative, that is, provides positive feedback on membrane potential variations, then the electrophysiological signature is distinctively different. This is, for instance, observed in a planar reduction of the Hodgkin–Huxley model augmented with an activating calcium current. The chief difference between the competitive and cooperative natures of the recovery variable is responsible for an alteration of the phase portrait that cannot be reproduced in the FitzHugh–Nagumo model and that calls for a generalized model that motivates the present paper.

We construct a highly degenerate pitchfork bifurcation (codimension 3) that is shown to organize excitability into five different types. The three first types correspond to the types of excitability extensively studied in the literature. They are all competitive in the sense that they involve only a region of the phase plane where the model recovery variable is purely competitive. In addition, the model reveals two new types of excitability (Types IV and V) that match the distinct electrophysiological signatures of conductance-based models of high density calcium channels. We prove that these two new types of excitability cannot be observed in a purely competitive model such as the FitzHugh–Nagumo model.

Global phase portraits of the proposed model are studied using singular perturbation theory, exploiting the timescale separation observed in all physiological recordings. An important result of the analysis is that Types IV and V excitable models exhibit a bistable range that persists in the singular limit of the model. This, in sharp contrast to Types I, II, and III. The result suggests the potential importance of Types IV and V excitability in bursting mechanisms associated to cooperative ion channels.

The paper is organized as follows. The studied planar model, its geometrical properties, and the underlying physiological concepts are presented in section 2. In section 3, we construct the pitchfork bifurcation organizing the model and unfold it into the five types of excitability. Types I, II, and III are briefly reviewed in section 4. Types IV and V are defined and characterized via phase plane and numerical bifurcation analysis in section 5. By relying on geometrical singular perturbations, we provide in section 6 a qualitative description of the phase plane of Types IV and V excitable models. Their peculiarities with respect to Types I, II, and III are particularly stressed. A summary and a discussion of our analysis are provided in section 7.

## 2. A mirrored FitzHugh–Nagumo model and its physiological interpretation. This paper studies the excitability properties of the planar model

$$\dot{V} = V - \frac{V^3}{3} - n^2 + I_{app}, \tag{2.1a}$$

$$\dot{n} = \epsilon(n_\infty(V - V_0) + n_0 - n), \tag{2.1b}$$

Transcritical organizing center



$$I_{app} < I^\star \qquad\qquad I_{app} = I^\star \qquad\qquad I_{app} > I^\star$$
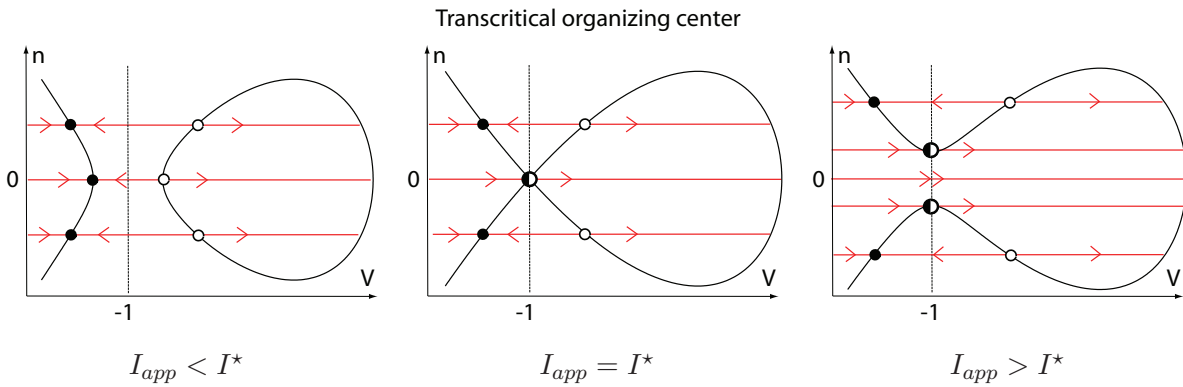
**Figure 1.** *V-nullcline (in black) and singular, i.e., $\epsilon = 0$, vector field (in red) of system (2.1) for different values of $I_{app}$. Stable fixed points are depicted as filled circles, unstable points as circles, and bifurcations as half-filled circles.*

where $n_\infty(V)$ is the standard Boltzman activation function[1]

$$(2.2) \qquad\qquad n_\infty(V) := \frac{2}{1 + e^{-5V}}.$$

The model is reminiscent of the popular FitzHugh–Nagumo model of neuronal excitability: equation (2.1a) describes the fast dynamics of the membrane potential $V$, whereas (2.1b) describes the slow dynamics of the "recovery variable" $n$ that aggregates the gating of various ionic channels.

The voltage dynamics (2.1a) are identical to the FitzHugh–Nagumo model, except that the quadratic term $n^2$ replaces the linear term $n$. This sole modification is central to the result of the present paper. The resulting nullcline $\dot{V} = 0$ "mirrors" along the $V$-axis the classical inverse N-shaped nullcline of the FitzHugh–Nagumo model, as illustrated in Figure 1. The figure illustrates the phase portrait of the model in the singular limit $\epsilon = 0$. The left and right phase portraits are the unfolding of the transcritical bifurcation organizing center (see, e.g., [32, pp. 104–105]) obtained for $I_{app} = I^\star := \frac{2}{3}$. This particular value will help us understand excitability mechanisms at work in the situation $I_{app} > I^\star$, illustrated in the right figure.

The recovery dynamics (2.1b) exhibit the familiar first-order relaxation of ionic current to the static sigmoid curve illustrated in Figure 2. For quantitative purposes, the numerator in the right-hand side of (2.2) can be picked larger than or equal to 2 without changing the underlying qualitative analysis. The parameters $(V_0, n_0)$ locate the relative position of the nullclines in the phase portrait. In particular, the region

$$(2.3) \qquad\qquad S_{n_0} := \{(V, n) \in \mathbb{R}^2 : n \in (n_0, n_0 + 2)\}$$

is attractive and invariant for the dynamics of system (2.1). The parameter $n_0$ slides up and down the "physiological window" of the recovery variable, whereas $V_0$ is the half-activation

---

[1]The factor 5 in the exponential ensures that the maximum slope of the activation function is larger than one, that is, $\max_{V \in \mathbb{R}} n'_\infty(V) > 1$, which is necessary to define $V^\star$ as in Figure 2 and for the geometrical construction in Figure 5.
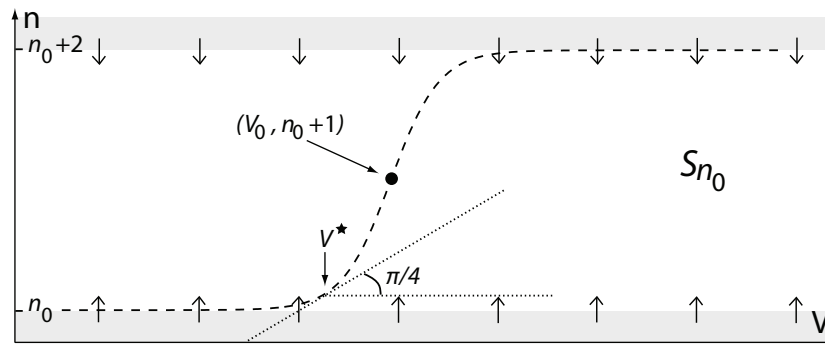
**Figure 2.** *Dependence of the n-nullclines (dashed line) of (2.1) on the parameters $n_0$ and $V_0$. The location of the nullcline in the phase plane determines an attractive invariant region $S_{n_0}$. At the voltage $V^\star$, the nullcline has a unitary slope.*

potential. The potential $V^\star < V_0$ is defined as the voltage at which $n_\infty(V - V_0)$ has unitary slope. We adopt the conventional notation $n$ for the recovery variable but will allow $n_0 < 0$, which makes the range of $n$ include negative values. This is purely for mathematical convenience and should not confuse the reader used to the physiological interpretation of a gating variable with range $[0, 1]$. For any value of $n_0$, the mathematical range $[n_0, n_0 + 2]$ of the recovery variable $n$ can be mapped to the physiological range $[0, 1]$ of a gating variable $\tilde{n}$ via the affine change of coordinate $\tilde{n} = \frac{n - n_0}{2}$.

**Competitive and cooperative excitability.** The recovery variable $n$ of model (2.1) is competitive in the half plane $n > 0$, that is, it provides a negative feedback on membrane potential variations, because

$$\frac{\partial \dot{V}}{\partial n} \frac{\partial \dot{n}}{\partial V} < 0.$$

In contrast, it is cooperative in the half plane $n < 0$, that is, it provides a positive feedback on membrane potential variations, because

$$\frac{\partial \dot{V}}{\partial n} \frac{\partial \dot{n}}{\partial V} > 0.$$

A consequence of that observation is that the recovery variable of model (2.1) is always competitive when $n_0 > 0$. The corresponding phase portrait is illustrated in Figure 3(A). It is reminiscent of the FitzHugh–Nagumo model and will recover known types of excitability. In contrast, $n$ is either competitive or cooperative when $n_0 < 0$. The corresponding phase portrait (Figure 3(B)) is distinctly different from the FitzHugh–Nagumo model and will lead to the novel types of excitability studied in this paper. The role of the proposed mirrored FitzHugh–Nagumo model is to study the transition from a purely competitive model to a model that is neither cooperative nor competitive through a single parameter $n_0$.

**The physiology behind competitive and cooperative behaviors.** Competitive and cooperative behaviors model different types of (in)activation gating variables in conductance-based models. When the recovery variable is purely competitive (Figure 3(A)), it models the acti-
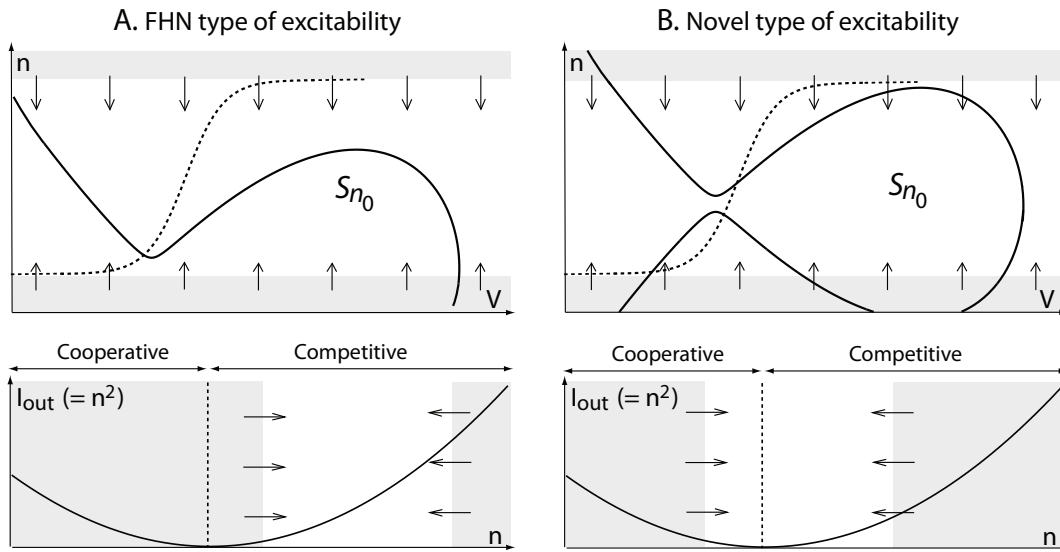
## A. FHN type of excitability          ## B. Novel type of excitability



**Figure 3.** *Nullclines (top) and outward ionic current $I_{out} = n^2$ (bottom) for different positions of the n-nullcline and the associated invariant region $S_{n_0}$. (A) When $S_{n_0}$ is fully contained in the half plane $n > 0$, the phase portrait is reminiscent of original FitzHugh–Nagumo model, and the outward ionic current is monotone increasing. The recovery variable has a purely competitive role. (B) When $S_{n_0}$ extends to the half plane $n < 0$, the phase portrait exhibits new characteristics. The outward ionic current is not monotone, corresponding to two antisynergistic (competitive and cooperative) roles of the recovery variable.*

vation (resp., inactivation) of an outward[2] (resp., inward) ionic current: a positive variation of $V$ induces a positive variation of $n$ and thus an *increase* of the total outward ionic current, i.e., $n^2$, which is monotone increasing in $S_{n_0}$. By contrast, when the recovery variable becomes cooperative (Figure 3(B)), its role is reversed: it models the activation (resp., inactivation) of an inward (resp., outward) ionic current: a positive variation of $V$ induces a positive variation of $n$ and thus a *decrease* of the total outward ionic current, which is now monotone decreasing.

The seminal Hodgkin–Huxley model includes only competitive slow gating variables: inactivation of sodium current and activation of potassium current. That is why the classical reduction of the Hodgkin–Huxley model leads to a FitzHugh–Nagumo type of phase portrait (Figure 3(A)). However, conductance-based models often include cooperative gating variables. An example of the latter is the activation of calcium currents included in many bursting conductance-based models (e.g., the R15 neuron of Aplysia's abdominal ganglion [27], thalamo-cortical relay and reticular neurons [24, 2], and the CA3 hippocampal pyramidal neuron [34]). Adding a calcium current in the Hodgkin–Huxley model is one natural way to obtain a reduced phase portrait as in Figure 3(B). This observation, first presented in [3] and reproduced in Figure 4, motivated the present study.

**3. A pitchfork bifurcation organizes different excitability types.** The model (2.1) has three free geometrical parameters $(I_{app}, n_0, V_0)$. The parameter $n_0$ is an additional parameter

---

[2]With the Hodgkin–Huxley convention, an outward current (i.e., flowing from the intracellular to the extracellular medium) is negative, and vice versa for inward currents.
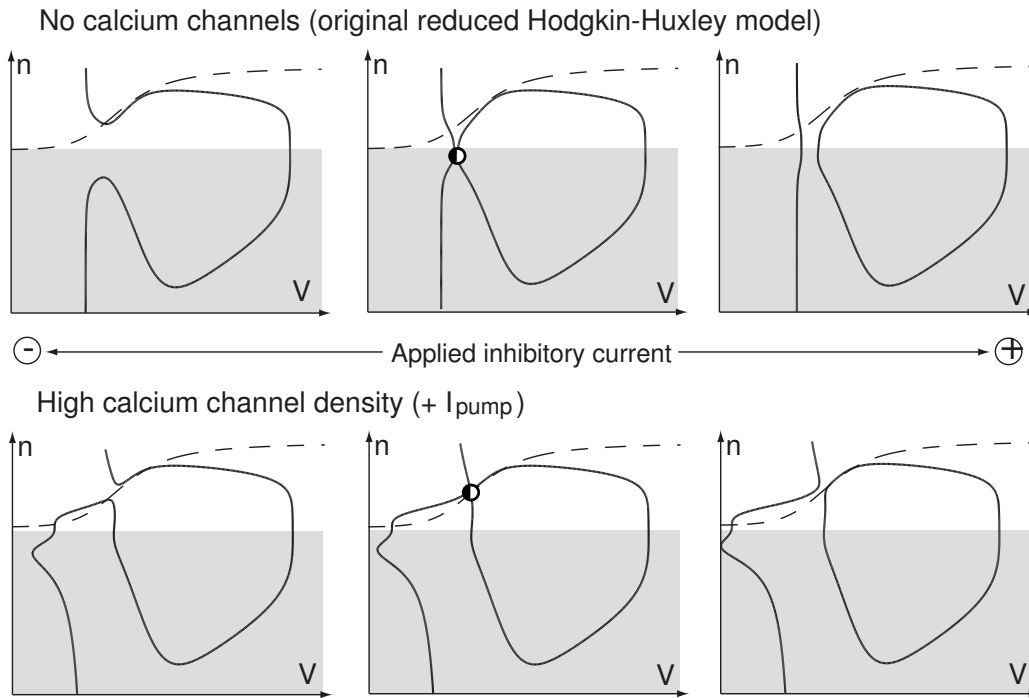
No calcium channels (original reduced Hodgkin-Huxley model)



$\ominus$ ←——————————— Applied inhibitory current ———————————→ $\oplus$

High calcium channel density (+ I$_{pump}$)



**Figure 4.** *Nullclines and transcritical singularities (half-filled circles) in reduced Hodgkin–Huxley model with and without calcium currents. In the original reduced Hodgkin–Huxley model, a transcritical singularity exists in the nonphysiological region of the phase plane (shaded area). The addition of a calcium current makes this bifurcation physiological.*
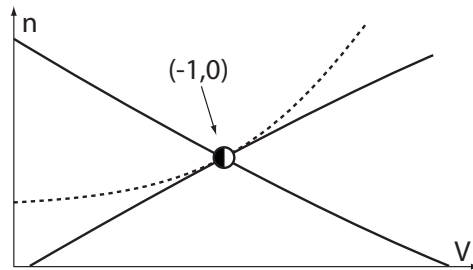


**Figure 5.** *V- and n-nullclines (solid and dashed lines, respectively) of model* (2.1) *for $I_{app} = I^\star$, $n_0 = n_0^\star(V_0)$, and $V^\star = -1$. The bifurcation obtained at the intersection is drawn as a half-filled circle.*

with respect to FitzHugh–Nagumo dynamics. The three parameters can be adjusted to create a codimension 3 bifurcation that will provide an organizing center for excitability.

The degenerate bifurcation is illustrated in Figure 5 and is constructed as follows:

1. The applied current is fixed at $I_{app} = I^\star$, imposing the existence of the singularly perturbed transcritical bifurcation at the $V$-nullcline self-intersection (cf. Figure 1, center).
2. We fix $n_0 = n_0^\star(V_0) := -n_\infty(-1-V_0)$ to force a nullcline intersection at the transcritical singularity at $(-1, 0)$.

3. We fix $V^\star = -1$, or, equivalently, $V_0 = V_0^\star := -1 + \frac{1}{5}\log\left(-6 + \sqrt{35}\right)$, so that the $n$-nullcline is tangent to the $V$-nullcline at the intersection.

A local normal form of the model (2.1) at this degenerate bifurcation is provided by the following lemma.

**Lemma 3.1.** *There exists an affine change of coordinates that transforms* (2.1) *into*

(3.1a)
$$\dot{v} = \frac{v^2(3-v)}{3} - \left(k(V_0)(v-u) + \delta_0\right)^2 + I_{app} - I^\star,$$

(3.1b)
$$\dot{u} = -\epsilon u + \mathcal{O}(v^2, \delta_0^2, u^2, vu, v\delta_0, u\delta_0),$$

*where* $k(V_0) := \frac{dn_\infty}{dV}(-1 - V_0)$ *is the slope of the activation function* $n_\infty(V - V_0)$ *at* $V = -1$, *and* $\delta_0 = n_0 + n_\infty(-1 - V_0)$.

*Proof.* The affine change of coordinates

$$\tilde{w} := n - \delta_0,$$
$$v = V + 1$$

transforms (2.1) into

$$\dot{v} = \frac{v^2(3-v)}{3} - (\tilde{w} + \delta_0)^2 + I_{app} - I^\star,$$

(3.2)
$$\dot{\tilde{w}} = \epsilon(n_\infty(v - 1 - V_0) - n_\infty(-1 - V_0) - \tilde{w}),$$

where $\delta_0$ is defined as in the statement of the lemma. Because $\dot{\tilde{w}}|_{v=\tilde{w}=0} = 0$, we extract the linear term in (3.2) and write

(3.3a)
$$\dot{v} = \frac{v^2(3-v)}{3} - (\tilde{w} + \delta_0)^2 + I_{app} - I^\star,$$

(3.3b)
$$\dot{\tilde{w}} = \epsilon(k(V_0)v - \tilde{w} + \mathcal{O}(v^2, v\tilde{w}, \tilde{w}^2)).$$

Finally, the linear transformation $u = v - \frac{\tilde{w}}{k(V_0)}$ transforms (3.3) into

$$\dot{v} = \frac{v^2(3-v)}{3} - (k(V_0)(v-u) + \delta_0)^2 + I_{app} - I^\star,$$
$$\dot{u} = -\epsilon u + \mathcal{O}(v^2, \delta_0^2, u^2, vu, v\delta_0, u\delta_0),$$

which proves the lemma. ∎

The dynamics (3.1) have an exponentially attractive center manifold that is tangent at $(v, u) = (0, 0)$ to center space $\{(v, u): \ u = 0\}$. Ignoring higher order terms, the dynamics on the center manifold is given by

(3.4)
$$\dot{v} = \left(1 - k(V_0)^2\right)v^2 - \frac{v^3}{3} - 2k(V_0)v\delta_0 - \delta_0^2 + I_{app} - I^\star.$$

**Codimension 2 transcritical bifurcation for $I_{app} = I^\star$, $n_0 = n_0^\star(V_0)$, $V_0 \neq V_0^\star$.** Fixing $I_{app} = I^\star$ (item 1) and $\delta_0 = 0$ (item 2), but $V_0 \neq V_0^\star$, we obtain from (3.4) the following relationships:

$$(3.5a) \qquad \dot{v}\Big|_{\substack{v=\delta=0 \\ I_{app}=I^\star \\ V_0 \neq V_0^\star}} = \frac{\partial \dot{v}}{\partial v}\Big|_{\substack{v=\delta=0 \\ I_{app}=I^\star \\ V_0 \neq V_0^\star}} = \frac{\partial \dot{v}}{\partial \delta_0}\Big|_{\substack{v=\delta=0 \\ I_{app}=I^\star \\ V_0 \neq V_0^\star}} = 0,$$

$$(3.5b) \qquad \frac{\partial^2 \dot{v}}{\partial v^2}\Big|_{\substack{v=\delta=0 \\ I_{app}=I^\star \\ V_0 \neq V_0^\star}} = 2\big(1 - k(V_0)^2\big) \neq 0,$$

$$(3.5c) \qquad \frac{\partial^2 \dot{v}}{\partial v \partial \delta_0}\Big|_{\substack{v=\delta=0 \\ I_{app}=I^\star \\ V_0 \neq V_0^\star}} = 2k(V_0) \neq 0,$$

where (3.5b) comes from the fact that, since $V_0 \neq V_0^\star$, $k(V_0) \neq 1$, whereas (3.5c) comes from the fact that $k(V_0) \neq 0$ for all $V_0 \in \mathbb{R}$. Relation (3.5) contains the defining conditions of a transcritical singularity (see, e.g., [32, page 367]). For any value of the perturbation parameter $\delta_0 \neq 0$, there are two fixed points that exchange their stability at the bifurcation for $\delta_0 = 0$. Figure 6(A),(C) illustrates this result. Note that we have to fix exactly two parameters (i.e., $I_{app}$ and $\delta_0$) to obtain (3.5), which confirms that the bifurcation described by (3.5) has codimension 2.

**Codimension 3 pitchfork bifurcation for $I_{app} = I^\star$, $n_0 = n_0^\star(V_0)$, $V_0 = V_0^\star$.** Adding the condition $V_0 = V_0^\star$ (item 3), we obtain the extra degeneracy condition

$$\frac{\partial^2 \dot{v}}{\partial v^2}\Big|_{\substack{v=\delta=0 \\ I_{app}=I^\star \\ V_0 \neq V_0^\star}} = 2\big(1 - k(V_0)^2\big) = 0,$$

and the associated bifurcation is in this case a codimension 3 pitchfork bifurcation (see, e.g., [32, page 367]). In this case, positive perturbation of $\delta_0$ leads to a unique stable fixed point, which splits into three fixed points, the outer stable and the central unstable, at the bifurcation (see Figure 6(B)).

**Unfolding in the plane $I_{app} = I^\star$.** The parameter chart in Figure 7 unfolds the pitchfork bifurcation in the plane $(V_0, n_0)$ for the fixed critical value $I^\star$. This bifurcation analysis reveals four qualitatively distinct regions denoted by I, II, IV, and V. The transition from Region I to Region II is through a saddle-node bifurcation at which the $n$-nullcline is tangent to the $V$-nullcline. Notice how the top right phase portrait is continuously deformed to the top left phase portrait in Figure 7. The transition from Region I to Region IV is through a transcritical bifurcation at which a saddle and a node exchange their stability. See how the top right phase portrait is continuously deformed to the bottom right phase portrait in Figure 7. A similar transition occurs from Region IV to Region V. Notice how the bottom right phase portrait is continuously deformed to the bottom left phase portrait in Figure 7. Finally, the transition
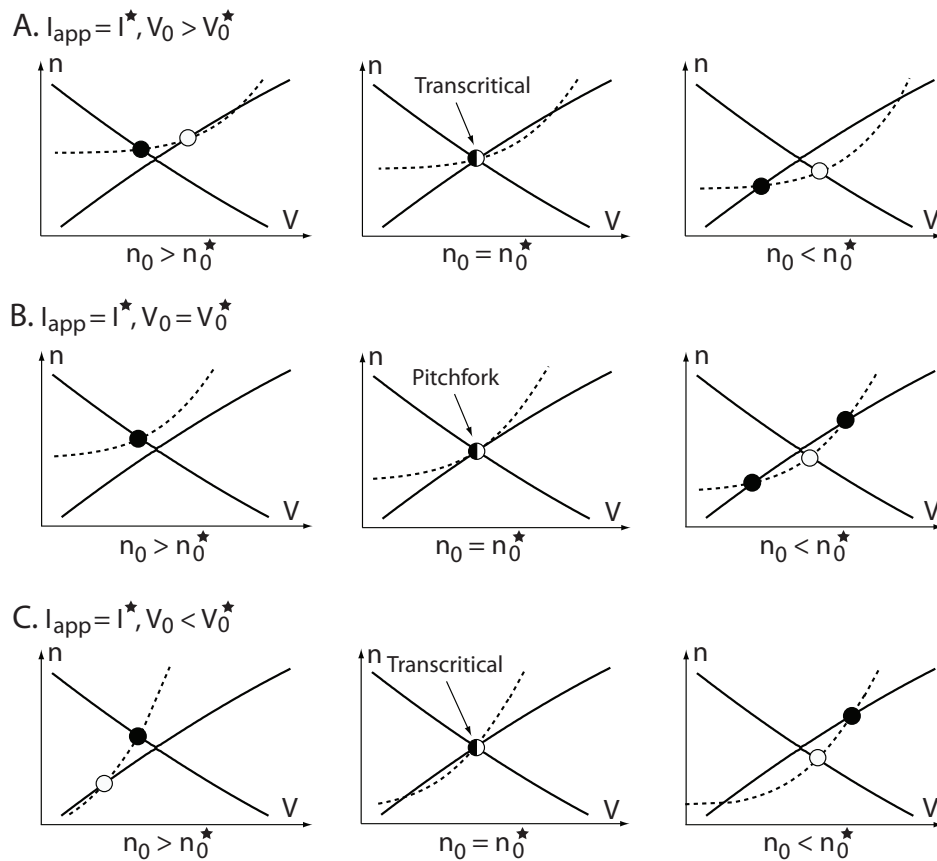
**Figure 6.** *Nullclines and fixed points of* (2.1) *for* $I_{app} = I^\star$, *different values of* $V_0$, *and with* $n_0$ *as the bifurcation parameter. Stable fixed points are drawn as filled circles, unstable points as circles, and bifurcations as half-filled circles.* (A),(C) *When* $V_0 < V_0^\star$ *or* $V_0 > V_0^\star$ *as* $n_0$ *decreases below* $n_0^\star(V_0)$, *a stable fixed point and an unstable fixed point exchange their stability in a codimension* 2 *transcritical singularity.* (B) *When* $V_0 = V_0^\star$, *the bifurcation degenerates into a codimension* 3 *pitchfork, at which a stable fixed point splits into two stable fixed points (outer) and an unstable fixed point (inner).*

from Region V to Region II is through a saddle-node bifurcation. Notice how the bottom left phase portrait is continuously deformed to the top left phase portrait in Figure 7.

Region III in Figure 7 is illustrated for future reference in the next section, but it should not be differentiated from Region II in the plane $I = I^\star$; i.e., there is no bifurcation associated to the transition from Region II to Region III.

**The pitchfork bifurcation organizes excitability.** The relevance of the unfolding in Figure 7 for excitability is that the different regions correspond to different types of excitability for $I_{app} > I^\star$. Regions I, II, and III correspond to Types I, II, and III excitability identified in the early work of Hodgkin [13] and extensively studied in the literature since then. Those are the only types of excitability that can be associated to purely competitive models (i.e., $n_0 > 0$), and they all have been studied in FitzHugh–Nagumo-type phase portraits. They are briefly reviewed in section 4. In contrast, Regions IV and V correspond to new types of excitability
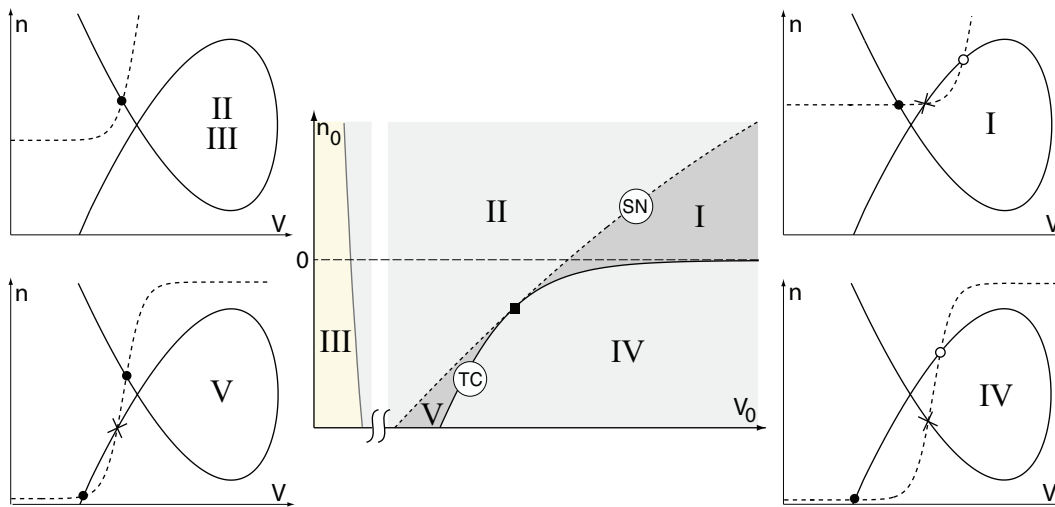
**Figure 7.** *Unfolding of the degenerate pitchfork bifurcation in the plane $I_{app} = I^\star$ and associated nullclines and fixed points. Stable fixed points are depicted as filled circles, whereas unstable points are depicted as circles. Saddle points are depicted as crosses. ■: pitchfork bifurcation. TC: transcritical bifurcation. SN: saddle-node bifurcation.*

that require the coexistence of competitive and cooperative ionic currents. They are studied in sections 5 and 6.

Our analysis assumes a timescale separation $\epsilon \ll 1$, reflecting the accepted strong separation between the *fast* voltage dynamics and sodium activation kinetics and the remaining *slow* gating kinetics. We focus on those bifurcations that persist in the singular limit $\epsilon \to 0$.

Figure 8 summarizes the different types of excitability studied in the next section and their main electrophysiological signatures.

The case $I_{app} < I^\star$ is less relevant for excitability models and therefore not studied in detail: for $I_{app} < I^\star$, there always exists a stable fixed point, and the only possible bifurcations are the two "vertical" saddle-nodes ($I_{SN,up}$ in Figures 9–11) in which the unstable fixed point of Type IV excitable systems and the stable up steady state of Type V excitable systems disappear, respectively. In this sense, this case corresponds to a condition of reduced excitability.

## 4. Three types of competitive excitability.

**Type I (SNIC).** Fixing the parameters $(V_0, n_0)$ in Region I of the parameter chart in Figure 7, the node and the saddle approach each other as the applied current $I_{app} > I^\star$ increases and eventually collide in a saddle-node bifurcation at the critical value $I_{app} = I_{SNIC}$, as depicted in Figure 8 (top right). Under the timescale separation assumption (i.e., $\epsilon \ll 1$), the center manifold of the bifurcation forms a homoclinic loop, as sketched in the figure. This bifurcation is commonly identified as a saddle-node on invariant circle (SNIC). As $I_{app}$ is further increased, the fixed point disappears and the system generates a periodic train of action potentials.

The excitability properties of model (2.1) near a SNIC bifurcation are commonly referred
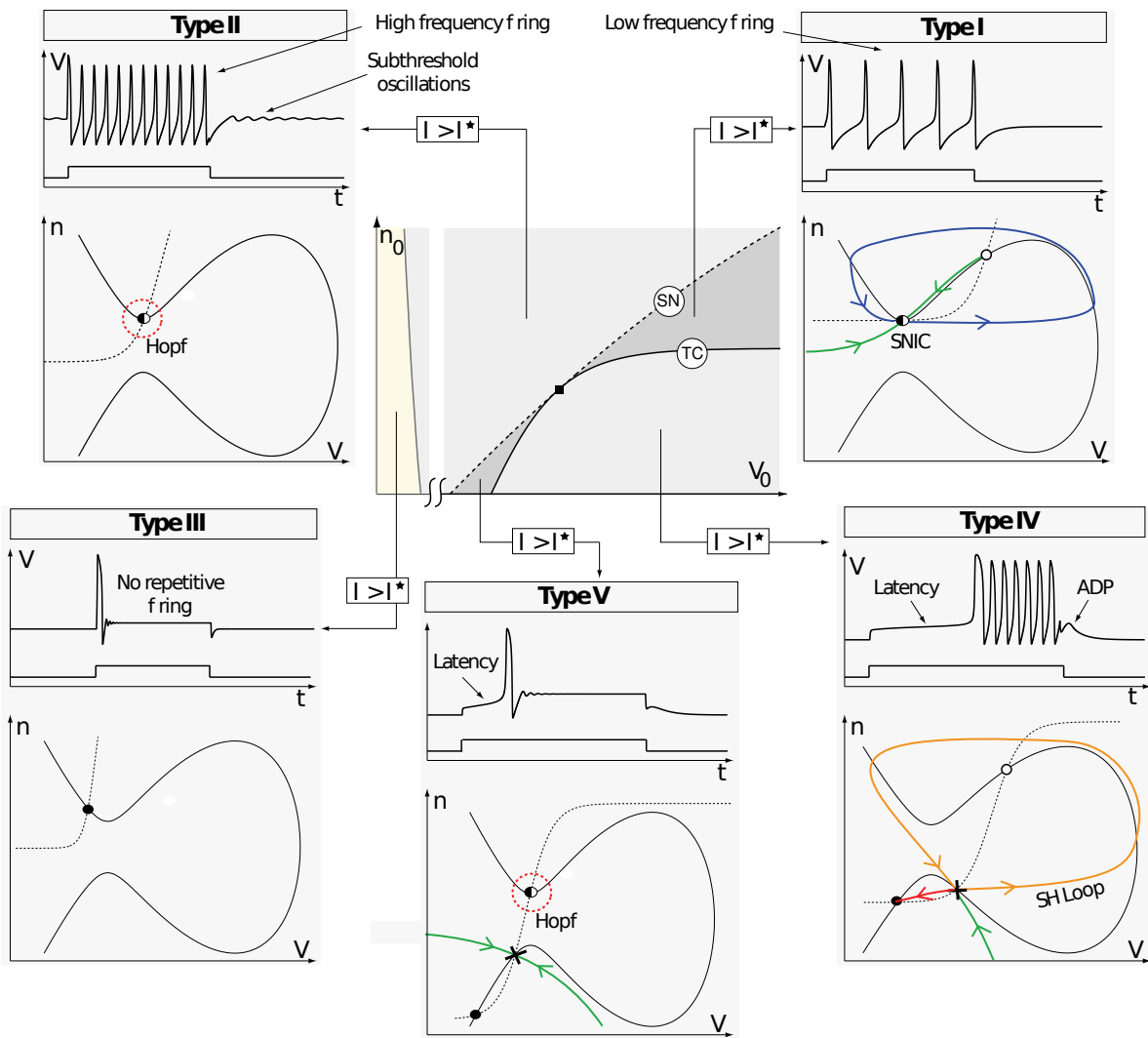
**Figure 8.** *Sketch of different types of excitable behaviors in the unfolding of the degenerate pitchfork bifurcation (■ in the central parameter chart) for $I_{app} > I^\star$ and $\epsilon \ll 1$. For each type, the typical voltage time course and the phase portrait are sketched. The abbreviation SNIC denotes the saddle-node on invariant circle bifurcation. Stable fixed points are depicted as filled circles, unstable points as circles, saddles as crosses, and bifurcations as half-filled circles. The stable manifold of saddle points is depicted in green. The center manifold of the SNIC bifurcation is depicted in blue. The saddle-homoclinic loop in Type IV is depicted in orange.*

to as Type I excitability (see, e.g., [4, section 3.4.4], [30], [15, section 7.1.3], and references therein). The main electrophysiological signatures associated to Type I excitability are as follows:

    *All-or-none spike.* The model has a well-defined threshold (i.e., $I_{app} = I_{SNIC}$) to generate action potentials. Above the threshold, the amplitude of the action potentials does not depend on the stimulus intensity.

    *Low frequency spiking.* The frequency of the limit cycle decreases to zero as $I_{app} \searrow$

$I_{SNIC}$. From a computational point of view, this property permits encoding the stimulus intensity in the oscillation frequency.

Examples of neurons exhibiting the electrophysiological signature of Type I excitability include thalamo-cortical neurons with inactivated T-type calcium current (depolarized steady-state) [38, Figure 3], isolated axons from Carcinus maenas [13, Class 1], regular spiking neurons in somatosensory cortex [33], and molluscan neurons [31].

**Type II (Hopf).** In Region II of the parameter chart in Figure 7, the nullclines intersect only once at a stable fixed point. As $I_{app}$ is increased, this fixed point loses stability in a Hopf bifurcation at $I_{app} = I_{Hopf}$, as illustrated in Figure 8 (top left). Above this critical input current, the system possesses a stable limit cycle surrounding the unstable fixed point.

Excitability properties associated to a Hopf bifurcation are well known and define Type II excitability (see, e.g., [4, section 3.4.4], [30], [15, section 7.1.3], and references therein). Fundamental electrophysiological signatures of Type II excitable systems include the following:

*No threshold.* When the bifurcation is supercritical, the amplitude of the limit cycle decreases to zero as $I_{app} \searrow I_{Hopf}$, which makes it hard to define a threshold for the generation of an action potential. Canard trajectories [35] are sometimes considered "soft" threshold manifolds between small and large amplitude action potentials.

*Subthreshold oscillations.* When the applied current is slightly below the bifurcation values (i.e., $I_{app} \lesssim I_{Hopf}$), the system trajectory relaxes to the fixed point with damped oscillations at the natural frequency of the Hopf bifurcation (i.e., the imaginary part of the eigenvalues at the bifurcation).

*No low frequency firing.* The oscillation frequency is (almost) independent of the injected current and is equal to or larger than the natural frequency of the Hopf bifurcation.

*Frequency preference.* Trains of small ($< I_{Hopf}$) amplitude inputs can induce spike if the intrastimulus frequency is resonant with the natural frequency of the Hopf bifurcation. This phenomenon is tightly linked to the presence of subthreshold oscillations and permits us to detect the presence of resonant harmonics in the stimulus.

*Postinhibitory spike.* Transient negative current can induce an action potential in Type II excitable systems.

Examples of neurons exhibiting the electrophysiological signature of Type II excitability include isolated axons from Carcinus maenas [13, Class 2], fast spiking neurons in somatosensory cortex [33], and alpha moto-neurons [25].

**Type III.** Type III excitability was only recently studied [7]. It can be thought of as a less excitable variant of Type II excitability. In Region III of Figure 7, the half-activation voltage $V_0$ is so negative that the stable focus never loses its stability as the applied current is increased. Nevertheless, the model is still excitable. For instance, as depicted in Figure 8 (bottom left), a positive current step instantaneously shifts the stable fixed point upright, and an originally resting trajectory is attracted toward the right branch of the $V$-nullcline before relaxing back to rest. On the contrary, if the applied current varies slowly, no action potential is generated.

Specific neurocomputational properties of Type III excitable systems have recently been highlighted in [7]:

*Slope detection.* Because a brutal variation of the applied current is necessary to excite the model, Type III excitable neurons act as slope detectors with a high temporal precision.

*Slope-based stochastic resonance.* In the presence of noise, Type III excitable models are most sensitive to the stimulus slope and frequency, rather than to its amplitude. The associated stochastic resonance phenomenon (slope-based stochastic resonance) exhibits distinctly different filtering properties with respect to the classical stochastic resonance in Types I and II excitable models.

Examples of neurons exhibiting the electrophysiological signature of Type III excitability include squid giant axons (revised model) [1], auditory brain stem [7], and isolated axons from Carcinus maenas [13, Class 3].

## 5. Two novel types of cooperative excitability.

**Type IV (singularly perturbed saddle-homoclinic).** As illustrated in the bottom right phase portrait of Figure 7, Type IV excitability is the first excitability type that involves the "mirrored" shape of the voltage nullcline in (2.1): the stable node and the saddle lie on the lower cooperative branch of the $V$-nullcline. In particular, the hyperpolarized stable steady state of Type IV excitable models lies in the cooperative region of the phase portrait, i.e., where

$$\frac{\partial \dot{V}}{\partial n} \frac{\partial \dot{n}}{\partial V} > 0.$$

As a consequence, excitability properties of this phase portrait cannot be studied in FitzHugh–Nagumo-like models.

Fixing the pair $(V_0, n_0)$ in Region IV of Figure 7, we obtain the bifurcation diagram illustrated in Figure 9 together with the associated phase portraits. The stable node loses stability in a saddle-node bifurcation at the critical value $I_{app} = I_{SN,down} > I^\star$. For $I_{app} > I_{SN,down}$, the model possesses a stable limit cycle that attracts all solutions (but the unstable focus). The spiking limit cycle disappears in a (singularly perturbed) saddle-homoclinic bifurcation at $I_{app} = I_{SH}$. The stable node attracts all solutions (but those on the stable manifold of the saddle) for $I_{app} < I_{SH}$. Further decreasing $I_{app}$ below $I_{SN,up}$, the unstable focus disappears in a saddle-node, letting the stable node be globally asymptotically stable. Based on geometrical singular perturbations, we provide in section 6 a global phase portrait analysis of Type IV excitable systems.

The chief electrophysiological signatures of Type IV excitable systems are as follows:

*Bistability.* Type IV excitable models are bistable in the parameter range $I_{SH} < I_{app} < I_{SN,down}$: a limit cycle attractor coexists with a stable fixed point.

*Spike-latency.* When the applied current is abruptly increased slightly above $I_{SN}$, the trajectory necessarily travels the narrow region between the nullclines. Since the vector field is small in that region, the first action potential is fired with a large latency.

*After-depolarization potential (ADP).* After the limit cycle has disappeared in the homoclinic bifurcation, the trajectory converges to rest by following the attractive branches of the voltage nullcline, thus generating robust ADPs (see [3]).

We stress that bistability, spike-latency, and ADPs are all direct consequences of the presence of a saddle point on the cooperative branch of the voltage nullcline: the basins of attraction of
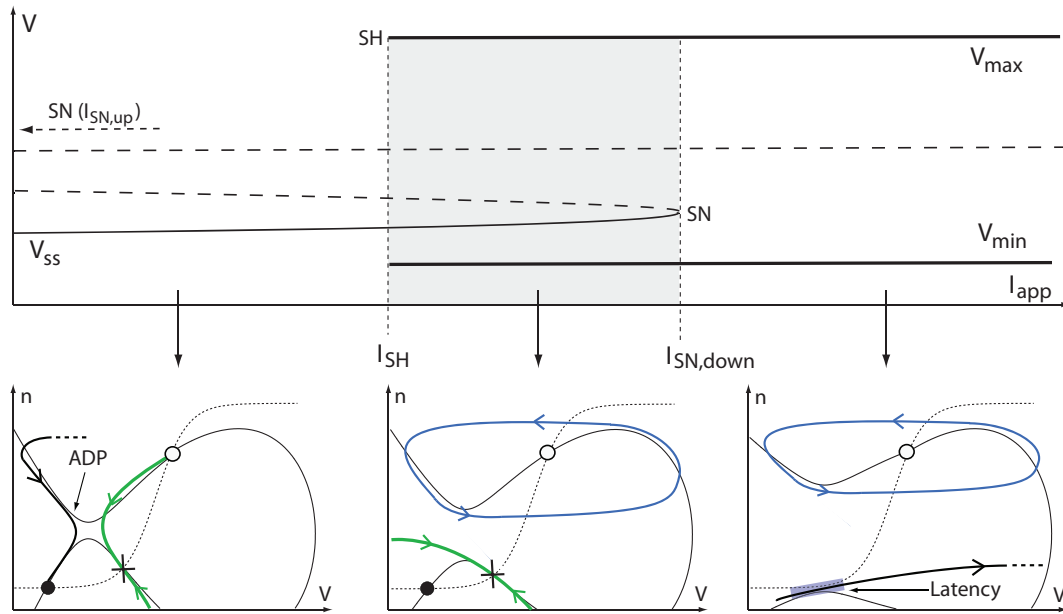
**Figure 9.** *Bifurcations in Type IV excitable systems. Top: Bifurcation diagram. Branches of stable fixed points are drawn as solid lines, those of unstable fixed points as dashed lines, and those of stable limit cycles as thick lines. SH denotes the saddle-homoclinic bifurcation and SN the saddle-node bifurcation. Bottom: Phase portraits. The stable manifold of saddle points is depicted in green. Unstable fixed points are depicted as circles, saddles as crosses, and stable fixed points as filled circles. Limit cycle attractors are depicted in blue. Sample trajectories are depicted as black oriented lines.*

the stable node and the limit cycle are separated by the stable manifold of the saddle; spike-latency reveals the "ghost" of the center manifold of the saddle-node bifurcation; ADPs are generated along the hyperbolic invariant structure provided by the saddle stable and unstable manifolds (see section 6 below).

Examples of neurons exhibiting the electrophysiological signature of Type IV excitability include subthalamic nucleus neurons [11], thalamo-cortical reticular and relay neurons with deinactivated T-type calcium current (hyperpolarized state) [14, 23], dopaminergic neurons [16, 8], and superficial pyramidal neurons [9].

**Type V (saddle-saddle).** Type V excitability relates to Type IV as Type III does to Type II: similarly to Type IV, the hyperpolarized stable steady state of Type V excitable models lies in the cooperative region of the phase plane. The distinct feature of the bottom left phase portrait of Figure 7 is the coexistence of two stable fixed points—a "down-state" and an "up-state." The saddle stable manifold separates the two attractors. As $I_{app}$ is decreased below $I^\star$, the up-state eventually loses its stability in a saddle-node bifurcation at $I_{SN,up}$, leaving the down-state globally asymptotically stable. Similarly, as $I_{app}$ is increased above $I^\star$, the down-state eventually disappears in a saddle-node bifurcation at $I = I_{SN,down}$. But the up-state itself eventually loses its stability in a Hopf bifurcation at $I_{app} = I_{Hopf}$. The Hopf bifurcation can either take place beyond the bistable range $[I_{SN,up}, I_{SN,down}]$, a situation illustrated in Figure 10, or take place within the bistable range $[I_{SN,up}, I_{SN,down}]$, in which
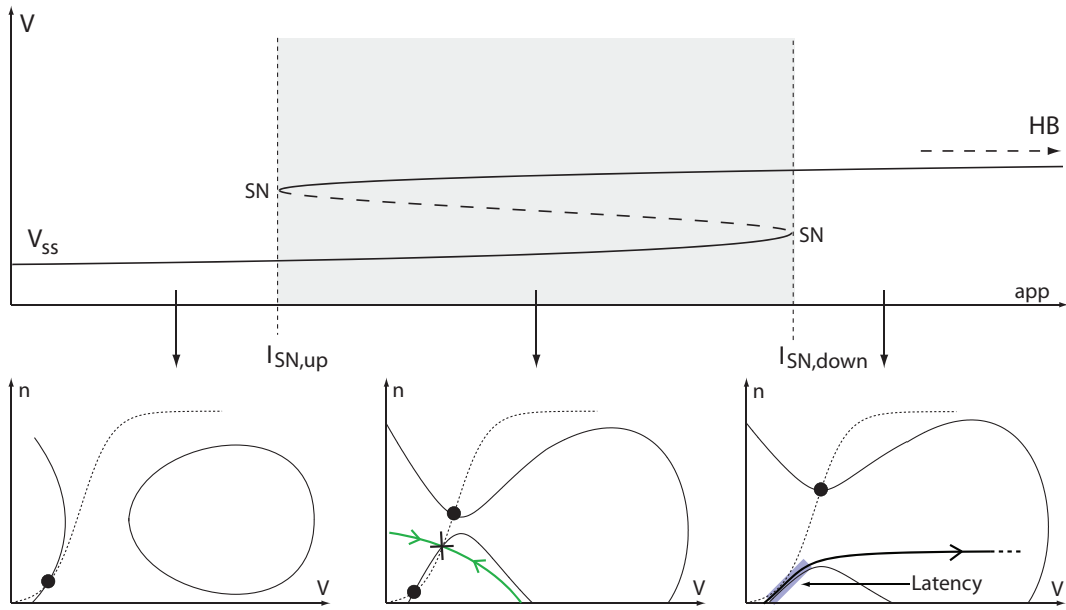
**Figure 10.** *Bifurcations in Type* V *excitable systems. Legend as in Figure* 9*, except HB denotes the Hopf bifurcation.*
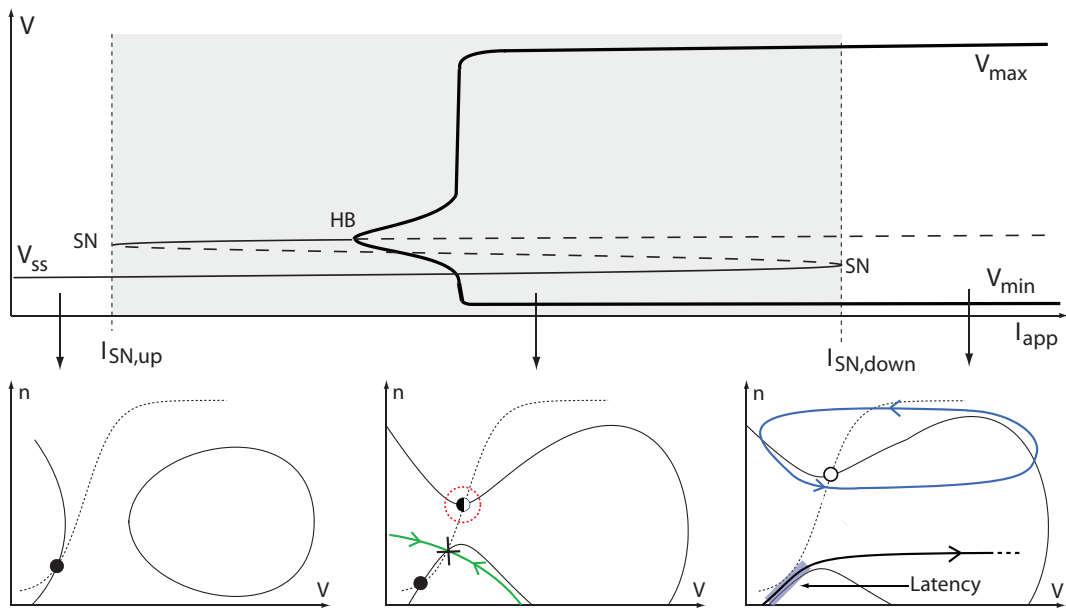


**Figure 11.** *Bifurcations in Type* V *excitable systems. Legend as in Figure* 9*, except HB denotes the Hopf bifurcation. The same bifurcation is depicted in the phase portrait as a half-filled circle.*

case, depending on $I_{app}$, the stable down-state coexists with either a limit cycle attractor or a stable fixed point, a situation illustrated in Figure 11.

The main electrophysiological signatures of Type V excitable models are similar to those

of Type IV and can be summarized as follows:

*Bistability.* Type V excitable models are bistable in the range $I_{SN,up} < I_{app} < I_{SN,down}$: a stable down-state coexists with an up-state attractor that can be either a stable fixed point or a stable limit cycle.

*Spike-latency.* Similarly to Type IV, the down-state loses stability in a saddle-node bifurcation on the lower (cooperative) branch of $V$-nullcline, leading to a long latency before the convergence to the up-state.

*Plateau potentials.* The up-state having a higher voltage with respect to the down-state, the transition between the two gives rise to plateau potentials either with or without spikes.

Examples of neurons exhibiting the electrophysiological signature of Type V excitability include olfactory bulb mitral cells [12] and striatal medium spiny neurons [37]. More examples are listed in the Scholarpedia Journal article [36].

## 6. Singularly perturbed global phase portrait analysis of Types IV and V excitable models.

Under the timescale separation assumption (i.e., $0 < \epsilon \ll 1$), Types IV and V excitable models exhibit four distinct signatures with respect to Types I and II: (i) the existence of a saddle-homoclinic bifurcation in Type IV; (ii) ADPs in Type IV; (iii) bistability in both Types IV and V; (iv) spike-latency in both Types IV and V. A global phase portrait analysis based on geometrical singular perturbations provides an analytical explanation for the occurrence of these signatures *solely* in Types IV and V.

### 6.1. Singularly perturbed saddle-homoclinic bifurcation and robust ADP generation in Type IV excitable models.

In this section we prove the existence of the saddle-homoclinic loop in Type IV excitable systems. We then rely on this analysis to provide a qualitative picture of the ADP generation mechanism in these models. In the remainder of the section we assume that the pair $(V_0, n_0)$ lies in Region IV of Figure 7.

We start by briefly recalling some basic results of geometrical singular perturbation theory, using (2.1) as an explicit example. The interested reader will find in [17] an excellent introduction to the topic and in [20, 22, 19, 18] some recent extensions on which we rely for the forthcoming analysis. The time rescaling $\tau := \epsilon t$ transforms (2.1) into the equivalent system

$$(6.1a) \qquad \epsilon \dot{V} = V - \frac{V^3}{3} - n^2 + I_{app},$$

$$(6.1b) \qquad \dot{n} = \epsilon(n_\infty(V - V_0) + n_0 - n),$$

which describes the dynamics (2.1) in the slow timescale $\tau$. In the limit $\epsilon = 0$, commonly referred to as the *singular limit*, one obtains from (2.1) and (6.1) two new dynamical systems: the *reduced dynamics*

$$(6.2a) \qquad 0 = V - \frac{V^3}{3} - n^2 + I_{app},$$

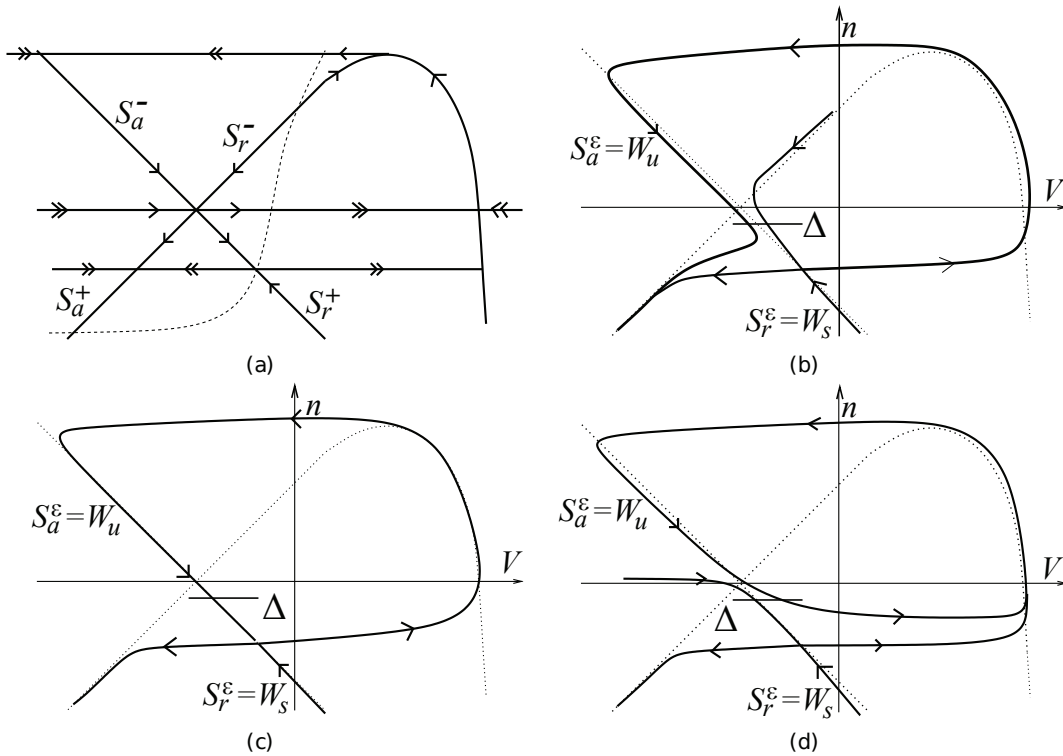$$(6.2b) \qquad \dot{n} = \epsilon(n_\infty(V - V_0) + n_0 - n),$$

**Figure 12.** *Phase-portrait of* (2.1) *for* $(n_0, V_0)$ *in region* IV *of the parameter chart in Figure* 7 *and different values of* $\epsilon$ *and* $I$. *(a) Fast-slow dynamics of* (2.1) *for* $\epsilon = 0$ *and* $I = I^\star$. *The attractive (resp., repelling) branches of the critical manifold* $S_0$ *above/below the transcritical singularity are denoted by* $S_a^+/S_a^-$ *(resp.,* $S_r^+/S_r^-$*). (b) Continuation of the slow attractive* $S_a^\epsilon$ *and repelling* $S_r^\epsilon$ *manifolds for* $\epsilon > 0$ *and* $I_{app} < I^\star + I_c(\sqrt{\epsilon})$, *where* $I_c(\sqrt{\epsilon})$ *is defined as in Theorem* 6.1. *(c) Continuation of* $S_a^\epsilon$ *and* $S_r^\epsilon$ *for* $\epsilon > 0$ *and* $I = I^\star + I_c(\sqrt{\epsilon})$. *(d) Continuation of* $S_a^\epsilon$ *and* $S_r^\epsilon$ *for* $\epsilon > 0$ *and* $I > I^\star + I_c(\sqrt{\epsilon})$.

which evolve in the slow timescale $\tau$, and the *layer dynamics*

$$(6.3a) \qquad \dot{V} = V - \frac{V^3}{3} - n^2 + I_{app},$$

$$(6.3b) \qquad \dot{n} = 0,$$

which evolve in the fast timescale $t$. Figure 12(a) depicts the fast-slow dynamics (6.2), (6.3). The main idea behind geometrical singular perturbation theory is to combine the analysis of the reduced and layer dynamics to derive conclusions about the behavior of the nominal system, i.e., with $\epsilon > 0$.

The reduced dynamics (6.2) is a dynamical system on the set

$$S_0 := \left\{ (V, n) \in \mathbb{R}^2 : \ V - \frac{V^3}{3} - n^2 + I_{app} = 0 \right\},$$

usually called the *critical manifold*. The points in $S_0$ are indeed critical points of the layer dynamics (6.3). More precisely, portions of $S_0$ on which $\frac{\partial \dot{V}}{\partial V}$ is nonvanishing are normally

hyperbolic invariant manifolds of equilibria of the layer dynamics, whose stability is determined by the sign of $\frac{\partial \dot{V}}{\partial V}$. Conversely, points in $S_0$ where $\frac{\partial \dot{V}}{\partial V} = 0$ constitute degenerate equilibria. In particular, the layer dynamics (6.3) exhibit, for $I_{app} = I^\star$, two degenerate equilibria.[3] As depicted in Figure 12(a) they are given by the self-intersection of the $V$-nullcline, which is the transcritical organizing center in Figure 1, and by the fold singularity at the maximum of the upper branch of the $V$-nullcline.

The basic result of geometrical singular perturbation theory, due to Fenichel [5], is that, for $\epsilon$ sufficiently small, nondegenerate portions of $S_0$ persist as nearby normally hyperbolic locally invariant manifolds $S^\epsilon$ of (2.1). More precisely, the *slow manifold* $S^\epsilon$ lies in a neighborhood of $S_0$ of radius $\mathcal{O}(\epsilon)$. The dynamics on $S^\epsilon$ is a small perturbation of the reduced dynamics (6.2). We point out that $S^\epsilon$ may not be unique but is determined only up to $\mathcal{O}(e^{-c/\epsilon})$ for some $c > 0$. That is, two different choices of $S^\epsilon$ are exponentially close (in $\epsilon$) to one another. Since the presented results are independent of the particular $S^\epsilon$ considered, we let this choice be arbitrary. The trajectories of the layer dynamics perturb to stable and unstable invariant foliations with basis $S^\epsilon$.

The analysis near degenerate points is more delicate and goes back to [28, 10, 21]. Only recently have some works treated this problem in its full generality for different types of singularities [19, 22, 18, 20]. Figure 12(b),(c),(d) sketches the extension of the attractive slow manifold $S_a^\epsilon$ after the fold point, and the three possible ways in which $S_a^\epsilon$ and the repelling slow manifold $S_r^\epsilon$ can continue after the transcritical singularity, depending on the injected current.

The result depicted in Figure 12 relies on the following analysis, adapted from [19].

Let $\Delta := \{(V, n) \in \mathbb{R}^2 : V_- \leq V \leq V_+, \ n = \rho\}$ be the section depicted in Figure 12, where $\rho < 0$ and $|\rho|$ is sufficiently small and $V_-, V_+$ are such that $\Delta \cap S_r^- \neq \emptyset$. For a given $\epsilon > 0$, let $q_{a,\epsilon} := \Delta \cap S_a^\epsilon$ and $q_{r,\epsilon} := \Delta \cap S_r^\epsilon$ be the intersections, whenever they exist, of, respectively, the attractive and repelling invariant submanifolds $S_a^\epsilon$ and $S_r^\epsilon$ with the section $\Delta$. The following theorem reformulates in a compact way the discussion contained in Remark 2.2 and section 3 of [19][4] for the system with inputs (2.1).

**Theorem 6.1 (adapted from [19]).** *Consider the system* (2.1). *Then there exist* $\epsilon_0 > 0$ *and a smooth function* $I_c(\sqrt{\epsilon})$, *defined on* $[0, \epsilon_0]$ *and satisfying* $I_c(0) = 0$, *such that, for all* $\epsilon \in (0, \epsilon_0]$, *the following assertions hold:*

1. *$q_{a,\epsilon} = q_{r,\epsilon}$ if and only if $I_{app} = I^\star + I_c(\sqrt{\epsilon})$.*
2. *There exists an open interval $A \ni I^\star + I_c(\sqrt{\epsilon})$ such that, for all $I \in A$, it holds that $\Delta \cap S_a^\epsilon \neq \emptyset$, $\Delta \cap S_r^\epsilon \neq \emptyset$, and*

$$\frac{\partial}{\partial I_{app}} (q_{a,\epsilon} - q_{r,\epsilon}) > 0.$$

Figure 12 illustrates this result.

**Remark 1.** *The function $I_c(\sqrt{\epsilon})$ is related to the function $\lambda_c(\sqrt{\epsilon})$ defined in* [19, *Remark 2.2*] *by $I_c(\sqrt{\epsilon}) := \epsilon \lambda_c(\sqrt{\epsilon})$. Similarly, given $\epsilon > 0$, the parameter $I_{app}$ appearing in Theorem*

---

[3]A third degenerate equilibria is at the minimum of the $V$-nullcline that is specular to the maximum with respect to the line $v = 0$, but it plays no dynamical role and is not considered here.

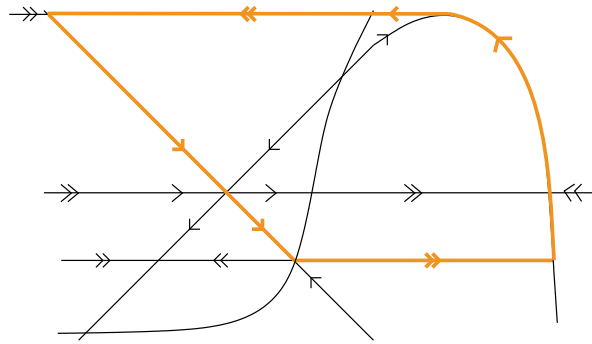[4]The first author is thankful to Prof. Szmolyan for his useful comments.

**Figure 13.** *Singularly perturbed nontrivial saddle-homoclinic connection near the transcritical singularity. This loop persists in the nonsingular limit.*

6.1 *is just the rescaling* $I_{app} = \epsilon\lambda + I^\star$ *of the parameter* $\lambda$ *appearing in* [19, *Remark* 2.2 *and Section* 3].

Theorem 6.1 implies the existence of the saddle-homoclinic bifurcation in the mirrored FitzHugh–Nagumo model (2.1) with parameters $(V_0, n_0)$ belonging to Region IV of Figure 7. In this case, as illustrated in Figure 12(b),(c),(d), the slow attractive manifold $S_a^\epsilon$ (resp., slow repelling manifold $S_r^\epsilon$) coincides with the unstable manifold $W_u$ (resp., stable manifold $W_s$) of the saddle point, as it can be proved via simple qualitative arguments. Thus, for $I_{app} < I^\star + I_c(\sqrt{\epsilon})$, the unstable manifold $W_u$ continues after the transcritical singularity on the left of $W_s$, toward the stable node. See Figure 12(b). For $I_{app} = I^\star + I_c(\sqrt{\epsilon})$, $W_u$ extends after the transcritical point to $W_s$, forming the saddle-homoclinic trajectory, as sketched in Figures 8 and 12(c). For $I_{app} > I^\star + I_c(\sqrt{\epsilon})$, the unstable manifold of the saddle $W_u$ continues after the transcritical singularity on the right of $W_s$ and spirals toward an exponentially stable limit cycle, whose existence can be proved with similar geometrical singular perturbation theory arguments (see, for instance, [20]). This situation is the one depicted in Figure 12(d).

The existence of the saddle-homoclinic bifurcation near the singular limit $\epsilon = 0$ is a direct consequence of the existence of a singular connection between the stable and unstable manifolds of the saddle, as sketched in Figure 13. The existence of the saddle-homoclinic bifurcation can be seen as the persistence of this singular saddle-homoclinic loop in the nonsingular dynamics. The same loop being absent in neuron models with an N-shaped nullcline, as discussed below, we identify the singularly perturbed saddle-homoclinic bifurcation sketched in Figure 8 (bottom right) as the signature of Type IV excitable models.

When $I_{app} < I^\star + I_c(\sqrt{\epsilon})$, the above analysis ensures the robust generation of ADPs. The trajectory relaxation to the stable fixed point is indeed guided by the normally hyperbolic attractive manifold $S_a^\varepsilon$. As illustrated in Figure 12(b), the voltage is not monotone as the trajectory slides along this manifold, corresponding to an ADP. The normal hyperbolicity of $S_a^\varepsilon$ ensures that the ADP generation is robust to external perturbations. Some consequences for the modeling of neurons exhibiting ADPs can be found in [3].

**Absence of singularly perturbed saddle-homoclinic bifurcation and ADPs in competitive models.** When the stable fixed point and the saddle belong to the upper N-shaped competitive branch of the voltage nullcline (i.e., Type I excitability), the model cannot ex-
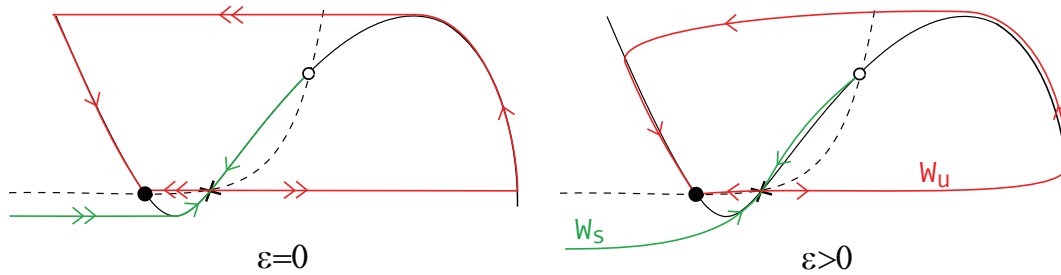
**Figure 14.** *Absence of a nontrivial singularly perturbed saddle-homoclinic connection around the N-shaped V-nullcline branch. Such a connection is also absent for sufficiently small $\epsilon > 0$.*

hibit saddle-homoclinic bifurcations. As sketched in Figure 14, in the fast-slow dynamics there are no nontrivial saddle-homoclinic connections. By persistence arguments [5, 20], this implies that the nontrivial intersection of the stable and unstable manifolds of the saddle is empty also away from the singular limit.

The prediction of singular perturbation theory of course does not contradict the existence of a saddle-homoclinic bifurcation in competitive models; it precludes it only for sufficiently small values of $\epsilon$. A well-known saddle-homoclinic bifurcation is described in the Morris–Lecar model [26] for the barnacle giant muscle fiber. The model is purely competitive, but a saddle-homoclinic bifurcation is possible around the N-shaped voltage nullcline (see, for instance, [4, section 3.4.3]). However, such a bifurcation cannot persist with a strong timescale separation, which suggests that it might be less relevant in the context of neuronal modeling.

The generation of ADPs must also be excluded when the stable fixed point belongs to the upper branch of the voltage nullcline. The relaxation to rest is indeed guided by the left attractive branch of the voltage nullcline, along which the voltage is monotone. ADPs can be generated within purely competitive models only by resorting to a nonphysiological state reset mechanism [15, section 8.3].

**6.2. Singularly perturbed bistability in Types IV and V excitable systems.** The geometrical singular perturbation machinery introduced above can be used to prove the persistence of bistability near the singular limit $\epsilon = 0$ for both Types IV and V excitable systems. The analysis is sketched in Figure 15. The underlying key ingredient is the existence of singularly perturbed separatrix $W_s^0$ passing by the saddle point. This object persists in the nonsingular limit as a normally hyperbolic saddle stable manifold $W_s^\epsilon$ that separates the stable down-state from the up-state attractor (see the bottom center plot in Figures 9, 10, and 11). The phase portraits in the nonsingular limit can all be deduced by the results in [20, 19, 18].

**Absence of singularly perturbed bistability in competitive models.** As opposed to Types IV and V, bistability is not observed in Types I, II, and III excitable models near the singular limit $\epsilon = 0$. For Type I, this can be deduced by the absence of a singularly perturbed separatrix (cf. Figure 14) and standard persistence arguments. For Type II, one can invoke the fact that the bistable range of the subcritical Hopf bifurcation shrinks to zero in the singular limit (see, for instance, [18, Theorem 3.1]). Type III excitable models are, by definition, always globally asymptotically stable.
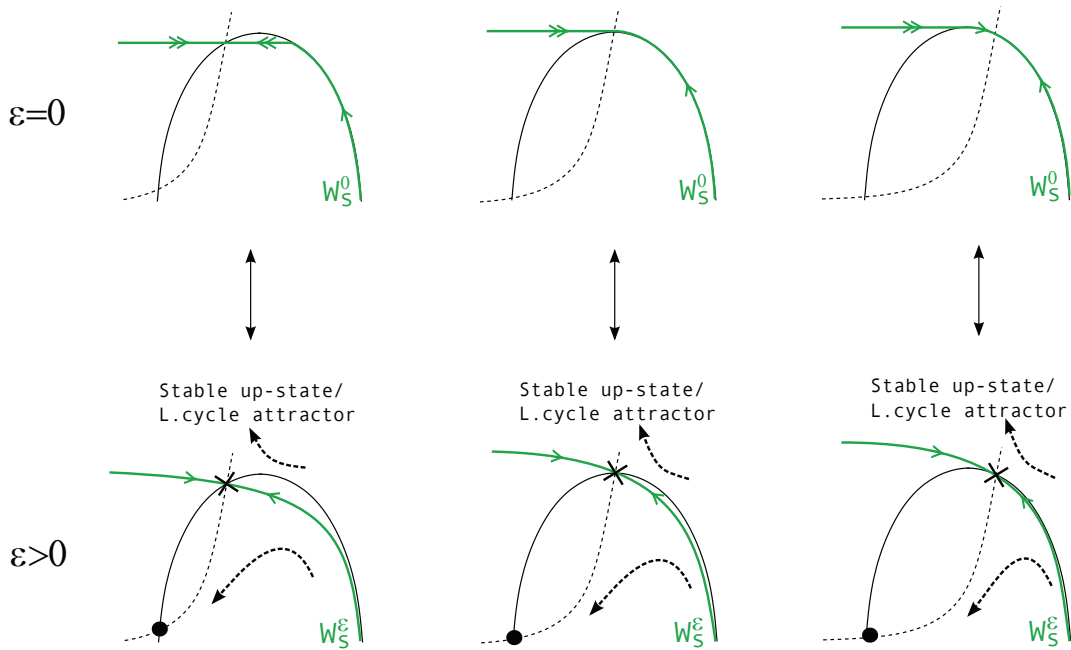
**Figure 15.** *Existence of a singularly perturbed saddle separatrix $W_s^0$ on the lower branch of the voltage nullcline in Types IV and V excitable systems for $I > I^\star$ and different nullcline intersections. Such an object persists in the nonsingular limit as the saddle stable manifold $W_s^\epsilon$, which separates the basin of attraction of the lower and upper attractors.*

**6.3. Singularly perturbed spike-latency in Types IV and V excitable systems.** Spike-latency appears when the trajectory travels the "ghost" of the center manifold of the saddle-node bifurcation. It is prominent in Types IV and V excitable models, since in these models this center manifold is attractive. Indeed, the recovery variable nullcline being strictly monotone increasing, the saddle-node bifurcation lies on the lower attractive branch of the voltage nullcline (see Figure 16). By standard persistence arguments, this implies that its center manifold $W_c^\epsilon$ is strongly attractive near the singular limit. A consequence of this attractiveness is that, after the bifurcation at $I_{app} = I_{SN}$, an originally resting trajectory is attracted toward the ghost of $W_c^\epsilon$ between the two nullclines, where the vector field magnitude is proportional to $I_{app} - I_{SN}$. The passage time thus diverges to infinity as $I_{app} \searrow I_{SN}$, corresponding to a prominent and robust spike-latency.

**Absence of singularly perturbed spike-latency in competitive models.** As opposed to Types IV and V, the saddle-node bifurcation of Type I excitable models lies on the upper repulsive (right) branch of the voltage nullcline (recall that the recovery variable nullcline is strictly monotone increasing). Hence, attractiveness of the bifurcation center manifold, and thus of its ghost, is lost near the singular limit. Even though for finite $\epsilon$ this center manifold can be attractive (see Figure 17), its ghost (between the two nullclines) does not attract an originally resting trajectory: the trajectory necessarily travels below the recovery variable nullcline where the vector field has finite magnitude independently of the distance from the bifurcation. These simple arguments show that competitive excitable models, and,
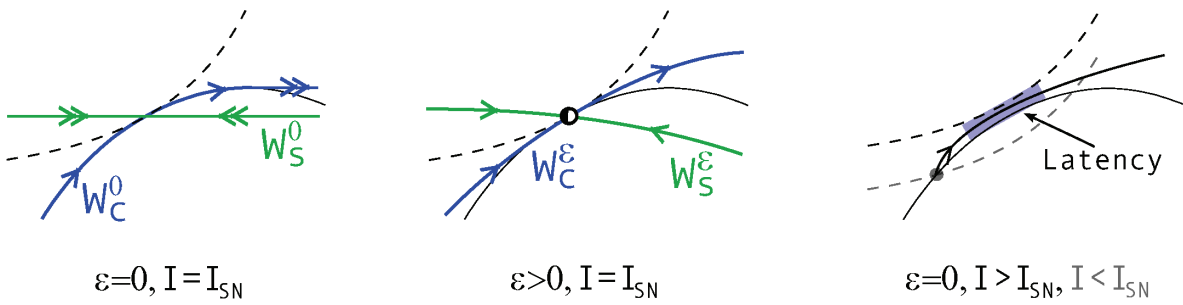
**Figure 16.** *Mechanism of spike-latency in Types IV and V excitable models. Left: Slow-fast dynamics near the saddle-node bifurcation. Center: Stable $W_s^\epsilon$ and center $W_c^\epsilon$ manifolds of the bifurcation for $\epsilon > 0$. Right: The ghost of $W_c^\epsilon$ (depicted as the blue rectangle) is attractive for $I > I_{SN}$ corresponding to prominent and robust spike-latency.*
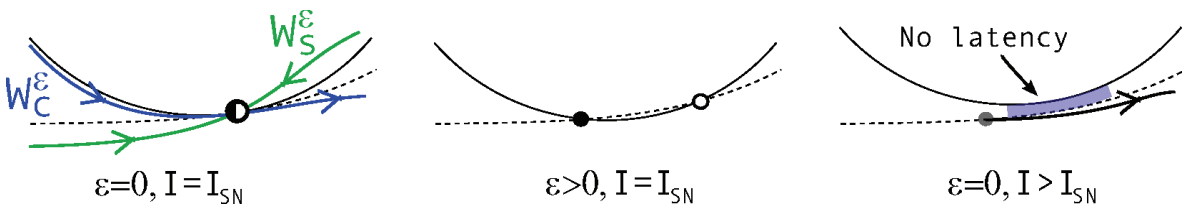


**Figure 17.** *Absence of spike-latency in Type I excitable models. Left: The saddle-node bifurcation in Type I excitable models with its center $W_c^\epsilon$ and stable $W_s^\epsilon$ manifolds. Center: The stable and the saddle fixed points before the bifurcation. Right: The ghost of $W_c^\epsilon$ (blue rectangle) after the bifurcation and the behavior of an originally resting trajectory.*

in particular, Type I excitable models, cannot exhibit spike-latency.

## 7. Discussion.

**Mirroring the FitzHugh–Nagumo equation accounts for cooperative gating variables.** Mirroring the FitzHugh–Nagumo equation was motivated by the inclusion, in a simple model of neuronal excitability, of the transcritical bifurcation recently observed in a planar reduction of the Hodgkin–Huxley model augmented with an activating calcium current. This heuristic geometrical construction is actually tightly linked with the underlying electrophysiology: in the upper FitzHugh–Nagumo-like part of the phase portrait, the model recovery variable is competitive, as it is in all reduced models derived from Hodgkin–Huxley dynamics; in the mirrored part, it is cooperative, accounting for cooperative gating variables, such as the activation of calcium current. To the best of our knowledge, this unified picture is not present in existing planar models of neuronal excitability, which are purely competitive.

**Cooperativity unravels a pitchfork bifurcation organizing old and new types of excitability.** The distinctive effects of cooperative gating variables on neuronal excitability are widely studied in high-dimensional conductance-based models and in *in vitro* recordings. However, these same signatures cannot be reproduced in competitive models, and the underlying dynamical mechanisms have remained obscure to date.

The unfolding of a pitchfork bifurcation organizing the proposed model reveals how the inclusion of cooperative variables changes neuronal excitability. The obtained parameter chart

recovers the three known types of (competitive) excitability and unmasks two novel types that we naturally defined as Types IV and V. The defining condition of Types IV and V excitability is cooperativity, i.e.,

$$\frac{\partial \dot{V}}{\partial n}\frac{\partial \dot{n}}{\partial V} > 0,$$

at the hyperpolarized stable steady state. This sole condition ensures the presence of the electrophysiological signatures of cooperative gating variables, particularly bistability.

**Competitive and cooperative excitability in higher-dimensional conductance-based models.** The planar model discussed in the present paper qualitatively captures an important switch from competitive to cooperative excitability. Electrophysiological recordings suggest that this switch actually occurs in the physiological range of many neurons. In a forthcoming publication, we will show that the switch indeed occurs in a number of published higher-dimensional conductance-based models. A qualitatively identical parameter chart to that in Figure 7 is found in those models, and the switch from competitive to cooperative excitability is traced through a transcritical bifurcation in the parameter space. In this sense, the planar model studied in the present paper is thought to capture a normal form reduction associated to a transcritical bifurcation that occurs in many quantitative conductance-based models of neurons.

**Bistability and bursting in singularly perturbed excitable models.** A distinct feature of Types IV and V excitable models with respect to the three other types is the existence of a finite range of bistability. Bistability has been described in the context of Types I and II excitability as well (see, e.g., [30]), but it was shown in section 6.2 that, in all these situations, the bistability range shrinks to zero as the timescale separation is increased. In contrast, the stable manifold of the saddle point that separates the two basins of attraction in Types IV and V excitability is a robust (hyperbolic) geometric object that persists in the singular limit. Because neurons do exhibit a pronounced timescale separation, the robustness of the bistable range in Types IV and V is thought to be an important feature of excitable models that are not purely competitive.

The relevance of bistability in excitable models lies in its relevance for model bursting. Bursting is typically the result of a slow adaptation variable that modulates the applied current across the bistability range, creating a hysteresis loop between the stable down-state and the up-state attractor. An important conjecture derived from our analysis is that bursting will persist near the singularly perturbed limit of model (2.1) only in Types IV and V excitability, that is, only in the presence of cooperative ionic channels. In other words, Types IV and V excitability would be the essential sources of bursting in singularly perturbed models.

**Methods.** The parameter charts in Figures 7 and 8 have been numerically drawn using MATLAB[5] and modified with the open-source vector graphics editor Inkscape.[6] Phase portraits were hand-drawn with Inkscape. The bifurcation diagrams in Figures 9, 10, and 11 have been obtained with the XPP environment.[7]

---

[5]http://www.mathworks.com
[6]http://inkscape.org
[7]http://www.math.pitt.edu/∼bard/xpp/xpp.html

## REFERENCES

[1] J. R. CLAY, D. PAYDARFAR, AND D. B. FORGER, *A simple modification of the Hodgkin and Huxley equations explains type 3 excitability in squid giant axons*, J. Roy. Soc. Interface, 5 (2008), pp. 1421–1428.

[2] A. DESTEXHE, D. CONTRERAS, M. STERIADE, T. J. SEJNOWSKI, AND J. R. HUGUENARD, *In vivo, in vitro, and computational analysis of dendritic calcium currents in thalamic reticular neurons*, J. Neurosci., 16 (1996), pp. 169–185.

[3] G. DRION, A. FRANCI, V. SEUTIN, AND R. SEPULCHRE, *A novel phase portrait for neuronal excitability*, PLoS ONE, 7 (2012), e41806.

[4] G. B. ERMENTROUT AND D. H. TERMAN, *Mathematical Foundations of Neuroscience*, Interdisciplinary Applied Mathematics 35, Springer, New York, 2010.

[5] N. FENICHEL, *Geometric singular perturbation theory*, J. Differential Equations, 31 (1979), pp. 53–98.

[6] R. FITZHUGH, *Impulses and physiological states in theoretical models of nerve membrane*, Biophys. J., 1 (1961), pp. 445–466.

[7] Y. GAI, B. DOIRON, V. KOTAK, AND J. RINZEL, *Noise-gated encoding of slow inputs by auditory brain stem neurons with a low-threshold K+ current*, J. Neurophysiol., 102 (2009), pp. 3447–3460.

[8] A. A. GRACE AND B. S. BUNNEY, *The control of firing pattern in nigral dopamine neurons: Burst firing*, J. Neurosci., 4 (1984), pp. 2877–2890.

[9] C. M. GRAY AND D. A. MCCORMICK, *Chattering cells: Superficial pyramidal neurons contributing to the generation of synchronous oscillations in the visual cortex*, Science, 274 (1996), pp. 109–113.

[10] R. HABERMAN, *Slowly varying jump and transition phenomena associated with algebraic bifurcation problems*, SIAM J. Appl. Math., 37 (1979), pp. 69–106.

[11] N. E. HALLWORTH, C. J. WILSON, AND M. D. BEVAN, *Apamin-sensitive small conductance calcium-activated potassium channels, through their selective coupling to voltage-gated calcium channels, are critical determinants of the precision, pace, and pattern of action potential generation in rat subthalamic nucleus neurons in vitro*, J. Neurosci., 23 (2003), pp. 7525–7542.

[12] P. HEYWARD, M. ENNIS, A. KELLER, AND M. T. SHIPLEY, *Membrane bistability in olfactory bulb mitral cells*, J. Neurosci., 21 (2001), pp. 5311–5320.

[13] A. L. HODGKIN, *The local electric changes associated with repetitive action in a non-medullated axon*, J. Physiol., 107 (1948), pp. 165–181.

[14] J. R. HUGUENARD AND D. A. PRINCE, *A novel T-type current underlies prolonged Ca(2+)-dependent burst firing in GABAergic neurons of rat thalamic reticular nucleus*, J. Neurosci., 12 (1992), pp. 3804–3817.

[15] E. M. IZHIKEVICH, *Dynamical Systems in Neuroscience: The Geometry of Excitability and Bursting*, MIT Press, Cambridge, MA, 2007.

[16] S. W. JOHNSON, V. SEUTIN, AND R. A. NORTH, *Burst firing in dopamine neurons induced by N-methyl-D-aspartate: Role of electrogenic sodium pump*, Science, 258 (1992), pp. 665–667.

[17] C. K. R. JONES, *Geometric singular perturbation theory*, in Dynamical Systems, Lecture Notes in Math. 1609, Springer, Berlin, 1995, pp. 44–120.

[18] M. KRUPA AND P. SZMOLYAN, *Extending geometric singular perturbation theory to nonhyperbolic points—fold and canard points in two dimensions*, SIAM J. Math. Anal., 33 (2001), pp. 286–314.

[19] M. KRUPA AND P. SZMOLYAN, *Extending slow manifolds near transcritical and pitchfork singularities*, Nonlinearity, 14 (2001), pp. 1473–1491.

[20] M. KRUPA AND P. SZMOLYAN, *Relaxation oscillation and canard explosion*, J. Differential Equations, 174 (2001), pp. 312–368.

[21] N. R. LEBOVITZ AND R. J. SCHAAR, *Exchange of stabilities in autonomous systems*, Stud. Appl. Math., 54 (1975), pp. 229–260.

[22] W. LIU, *Exchange lemmas for singular perturbation problems with certain turning points*, J. Differential Equations, 167 (2000), pp. 134–180.

[23] D. A. MCCORMICK AND T. BAL, *Sleep and arousal: Thalamocortical mechanisms*, Ann. Rev. Neurosci., 20 (1997), pp. 185–215.

[24] D. A. MCCORMICK AND J. R. HUGUENARD, *A model of the electrophysiological properties of thalamocortical relay neurons*, J. Neurophysiol., 68 (1992), pp. 1384–1400.

[25] C. MESSINA AND R. COTRUFO, *Different excitability of type* 1 *and type* 2 *alpha-motoneurones: The recruitment curve of H- and M-responses in slow and fast muscles of rabbits*, J. Neurological Sci., 28 (1976), pp. 57–63.

[26] C. MORRIS AND H. LECAR, *Voltage oscillations in the barnacle giant muscle fiber*, Biophys. J., 35 (1981), pp. 193–213.

[27] R. E. PLANT AND M. KIM, *Mathematical description of a bursting pacemaker neuron by a modification of the Hodgkin-Huxley equations*, Biophys. J., 16 (1976), pp. 227–244.

[28] L. S. PONTRYAGIN, *Asymptotic behavior of solutions of systems of differential equations with a small parameter in the derivatives of highest order*, Izv. Ross. Akad. Nauk Ser. Mat., 21 (1957), pp. 605–626.

[29] J. RINZEL, *Excitation dynamics: Insights from simplified membrane models*, in Fed. Proc., Vol. 44, 1985, pp. 2944–2946.

[30] J. RINZEL AND G. B. ERMENTROUT, *Analysis of neural excitability and oscillations*, in Methods in Neuronal Modeling, MIT Press, Cambridge, MA, 1989, pp. 135–169.

[31] S. SESSLEY AND R. J. BUTERA, *Evidence for "type* I*" excitability in molluscan neurons*, in Engineering in Medicine and Biology, Proceedings of the 24th Annual Conference and the Annual Fall Meeting of the Biomedical Engineering Society (EMBS/BMES Conference), Vol. 3, IEEE, Washington, DC, 2002, pp. 1966–1967.

[32] R. SEYDEL, *Practical Bifurcation and Stability Analysis*, 3rd ed., Interdisciplinary Applied Mathematics 5, Springer-Verlag, New York, 2010.

[33] T. TATENO, A. HARSCH, AND H. P. C. ROBINSON, *Threshold firing frequency–current relationships of neurons in rat somatosensory cortex: Type* 1 *and type* 2 *dynamics*, J. Neurophysiol., 92 (2004), pp. 2283–2294.

[34] R. D. TRAUB, R. K. WONG, R. MILES, AND H. MICHELSON, *A model of a CA*3 *hippocampal pyramidal neuron incorporating voltage-clamp data on intrinsic conductances*, J. Neurophysiol., 66 (1991), pp. 635–650.

[35] M. WECHSELBERGER, *Canards*, Scholarpedia J., 2 (2007), p. 1356.

[36] C. WILSON, *Up and down states*, Scholarpedia J., 3 (2008), p. 1410.

[37] C. J. WILSON AND P. M. GROVES, *Spontaneous firing patterns of identified spiny neurons in the rat neostriatum*, Brain Res., 220 (1981), pp. 67–80.

[38] X. J. ZHAN, C. L. COX, J. RINZEL, AND S. M. SHERMAN, *Current clamp and modeling studies of low-threshold calcium spikes in cells of the cat's lateral geniculate nucleus*, J. Neurophysiol., 81 (1999), pp. 2360–2373.